## Clay-containing polymeric nanocomposites, characterization, high pressure dilatometry

Utracki, L. A.



*Proceedings of the American Society for Composites / Joint US-Canada Conference on Composites, 2011-09-26*

# Clay-containing polymeric nanocomposites; Characterization, high pressure dilatometry

L. A. Utracki, NRCC/IMI, 75 de Mortagne, Boucherville, QC, Canada J4B 6Y4

*


## ABSTRACT

In structural clay-containing polymeric nanocomposites (CPNC) ca. 2 – 5 wt% clay is dispersed in polymer matrix: thermoplastic, thermoset or elastomeric. Since most clay/polymer systems are antagonistically immiscible, in analogy to immiscible polymer blends, a two-step compatibilization is required: (1) intercalation of clay into organoclay and (2) addition of functional compatibilizer(s). The volume of these compatibilizing species usually is larger than that of clay itself. These additives affect the thermodynamic, rheology and other performance characteristics of CPNC. Since the system is immiscible, i.e., sensitive to stresses during the compounding and forming stages, the reproducibility of behavior may be a problem. Furthermore, from the chemical and physical points of view the natural and synthetic clays are complex. The purified natural clay may contain 2-5 wt% contaminants (humic derivatives, quartz, gypsum, dolomite, ...), whereas the synthetic ones may be a mixture of different crystallographic forms (e.g., lamellar and needle-like). Both types of clay have polydispersed platelets shape and size. Accordingly, characterization of CPNC should start with that of clay, its platelet size, their inherent dispersibility (absence of interlamellar crystalline welding) and presence of contaminants. CPNC are being characterized by the rheological methods in the solid and molten state. Their mechanical, barrier, dielectric and other properties are determined following the standard methods. However, the use of the high pressure dilatometry (HPD) is relatively rare, even when this is the simplest way for determining the free volume and the thermodynamic interaction parameters as well as the key engineering quantities: the thermal expansion and compressibility coefficients. The HPD measurements are important, especially in view of the kinetic nature of transitions (vitrification, crystallization) that stretches into the non-equilibrium melt. An overview of the method and results obtained for CPNC with amorphous or semi-crystalline polymeric matrices are described.


## CHARACTERIZATION OF CLAY

The clay-containing polymeric nanocomposites (CPNC) are dispersions of clay in a polymer. For good performance the exfoliation is desired. In industrial manufacture of structural CPNC crystalline clay, natural or synthetic, is used. The clay platelets are 0.7 – 1.7 nm thick with the aspect ratio: $p$ = diameter/thickness = 20 – 6000 [1]. [1] The natural clays are contaminated with (1) organic (*e.g.*, humic substances, HS), (2) parasitic clays

* *L. A. Utracki*, NRCC/IMI, 75 de Mortagne, Boucherville, QC, Canada J4B 6Y4

(*e.g.*, amorphous or non-expandable) and (3) particulate minerals (quartz, sand, silt, feldspar, gypsum, orthoclase, apatite, calcite, dolomite, biotite, etc).

CPNC manufacture involves melt compounding in a single or twin-screw extruder (SSE or TSE, respectively) in the shear or extensional flow field. Dispersing in extensional flow is more energy-efficient, generates better dispersive and distributive mixing, is performed in a more uniform flow field at lower temperatures and it does not re-aggregates solid particles as the shear field does. Some years back the extensional flow mixer (EFM) and its dynamic version, DEFM were developed. These devices may be attached to a SSE or TSE, or it may be used as stand-alone [2]. [2] The key requirement for good CPNC clay is its ability to exfoliate, which is related to the ionic imbalance of the crystalline layers, compensated by hydrated ions in the interlayer galleries. The most important (natural or synthetic) exfoliating clays are: montmorillonite (MMT), hectorite (HT), and saponite (SP). These minerals have an octahedral layer (Oc) sandwiched between two tetrahedral (Tc) ones. The synthetic clays are classified as [3]: [3]

- *Semi-synthetic, prepared in a reaction of natural mineral with salt.*
- *Synthetic, formed in a reaction between metal salts or oxides.*
- *Templated, starting with organic templates, which after synthesis may be pyrolyzed.*

In the recent VAMAS TWA-33 project three types of sodium-clays were studied [4]: [4] (1) the natural MMT, Cloisite®-$Na^+$ (C-$Na^+$), (2) the semi-synthetic fluoro-hectorite, Somasif ME-100, and (3) the synthetic fluoro-tetrasilicic mica, Topy-$Na^+$. Their properties are listed in Table I.

Table I. Properties of the sodium-clays.

| Property | C-Na+ | ME-100 | Topy-Na+ |
|---|---|---|---|
| Specific density, g/mL | 2.86 | 2.6 | 2.6 |
| Interlayer spacing, d001 (nm) | 1.17 | 0.95 | 1.23 |
| Platelets thickness, nm | 0.96 | 0.91 | |
| CEC (meq/g) | 0.92 | 1.2 | 0.80 |
| Nominal aspect ratio, p (-) | 280 | ≤ 6000 | ≤ 5000 |

The clays were characterized for platelet shape, size, chemical composition and impurities. The test methodology and results are published in [4]. Example of ME-100 images is shown in Figure 1. The number and weight average values of the platelet length and the orthogonal width (subscripts *n* and *w*, respectively) are listed in Table II. The average clay platelet dimensions in three orthogonal directions are: thickness $t \approx 1$ nm, width $W \approx 20 – 4000$ nm, length $L \approx 30 – 6000$ nm, with the nearly universal ratio $L/W \approx 1.5 \pm 0.1$. The distribution of clay platelet size is nearly Gaussian.

Table II. Statistical analysis of three clays.

| Clay | Length L (nm) | | Width, W (nm) | | Ratios | |
|---|---|---|---|---|---|---|
| | $L_n$ | $L_w$ | $W_n$ | $W_w$ | $(L/W)_n$ | $(L/W)_w$ |
| Natural, C-$Na^+$ | 290 | 350 | 183 | 219 | 1.58 | 1.60 |
| Semi-synthetic, ME-100 | 872 | 1097 | 572 | 743 | 1.52 | 1.48 |
| Synthetic, Topy-$Na^+$ | 1204 | 1704 | 761 | 1186 | 1.58 | 1.44 |
| Error | | | | | ± 0.2 | ± 0.2 |

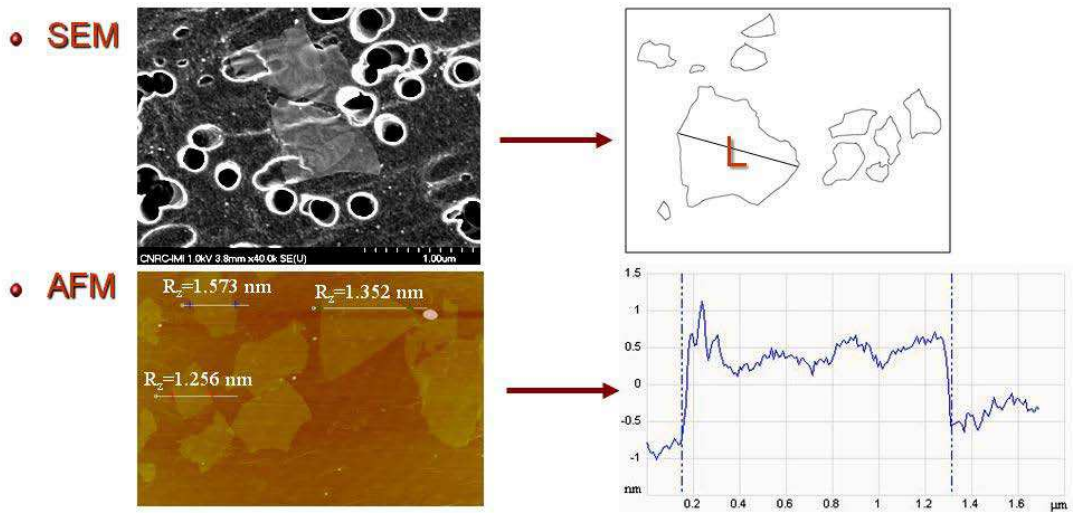


Figure.1. Scanning electron microscopy (SEM) and atomic force microscopy (AFM) images of Somasif ME-100 platelets. As an example, the platelet length is indicated as L; the width is taken as the largest perpendicular to L platelet size [4].

Chemical analysis of clays was obtained by the Energy-dispersive X-ray (EDX) analysis in SEM. Since clay particles may have locally different composition, ca. 30 particles were sampled at least five locations, each. Results are listed in Table III.

Table III. Elemental composition of C-$Na^+$ and ME-100 clays [4].

| Source | C-$Na^+$ | ME-100 |
|---|---|---|
| Nominal | $[Al_{3.34}Mg_{0.66}Na_{0.66}](Si_8O_{20})(OH)_4$ | $(NaF)_{2.2}(MgF_2)_{0.1}(MgO)_{5.4}(SiO_2)_8$ |
| Found | $[Al_{2.9}Fe_{0.6}Mg_{0.35}Na_{0.72}](Si_8O_{20})(OH)_4$ | $(NaF)_{0.94}(MgF_2)_{2.3}(MgO)_{2.7}(SiO_2)8$ |
| O | 21.10 | 22.80 |
| Na | 0.72 | 0.94 |
| Mg | 0.35 | 5.00 |
| Al | 2.90 | -- |
| Si | 8.00 | 8.00 |
| Fe | 0.63 | -- |
| F | -- | 5.50 |

There are three principal sources for variability of composition in the natural C-$Na^+$ and semi-synthetic ME-100 clays: (a) non-uniform atomic substitution in the crystalline cells, (b) reported tendency of natural clays to vary composition with each particle, (c) presence of impurities. Owing to the latter, in natural clays the scatter of ±15% has been observed. Variability in ME-100 is larger than the error of measurements what also reflects on the local variation of composition. The chemical heterogeneity may cause batch-to-batch variability of the mechano-chemical sensitivity during CPNC compounding, degradability, weatherability, sensitivity or lack of it toward antioxidants and stabilizers, etc.

Purification of natural clays into polymer-grade materials is a complex process with about 300 steps. The patents specify that the product should contain ≤ 5 wt% of impurities, > 300 nm large [5]. [5] The following minerals were identified in C-$Na^+$: vermiculite, quartz, cristobalite, rutile, albite, microcline, aragonite, vaterite, dolomite, gypsum, anhydrite, alunite and sylvite. As expected, the semi-synthetic ME-100 contained traces of contaminants brought in with talc: vermiculite and gypsum. The presence of

particulates, incompatible with the matrix polymer, reduces mechanical performance as well as the barrier performance.

## CPNC

Clay dispersion in SSE or TSE resembles that of polymer alloys and blends (PAB), thus thermodynamic interactions and complex flow field (shear, chaotic and extensional mixing) are of key importance [6, 7]. [6, 7] In CPNC, the interactions are modified by intercalant, and compatibilizers, as well as by clay high surface energy, which leads to adsorption-&- solidification of the organic molecules. Such adsorption has been observed using the surface force analyzer (SFA) and the neutron scattering methods [8-11].[8, 9, 10, 11] Also molecular dynamics computations predict formation of the solidified layer [12-14].[12, 13, 14] Thus, in the $z$-direction perpendicular to clay surface there are two layers with reduced molecular dynamics: $z_1 \approx$ 2-9 nm thick solid layer followed by $z_2 - z_1$ = 100-120 nm thick layer where molecular mobility progressively increases from $z_1$ to $z_2$. Luengo *et al.* determined that on a freshly cleaved mica flake thickness of the first and second layer were 5-6 and 100 nm, respectively. Thus, the polymer melt bulk behavior was observed at $z_2 \geq$ 110 nm.

The CPNC tensile and flexural properties (*i.e.*, modulus or strength) are proportional to each other [15]. [15] At low loadings the relative modulus follows the linear dependence:

$$E_R \equiv E_c / E_m = 1 + a_w w(wt\%) \tag{1}$$

(subscripts $c$ and $m$ stand for composite and matrix, respectively). For CPNC with PA or PP matrix $a_w \approx$ 0.2, thus at 5 wt% clay the modulus doubles. In elastomers the effect is larger: $a_w \approx$ 0.7. Factorial analyses indicate that $E_R$ is a linear function of the interlayer spacing, $d_{001}$. The tensile strength theory predicts that relative strength:

$$\sigma_R \equiv \sigma_c / \sigma_m \leq 1 + \phi_f \left( \sigma_f / \sigma_m - 1 \right) \tag{2}$$

where $\phi_f$ is clay volume fraction. Because of polymer solidification on clay, the experimental $\sigma_R$ values for CPNC with PA-6 or PP are 9 and 5 times larger than predicted by eq. 2. At low clay content, the rigidity and strength linearly increases with exfoliation.

## HIGH PRESSURE DILATOMETRY (HPD)

### TRANSITIONS

Within the temperature range from 0 (K) to decomposition the polymers undergo several transitions. Of these, the melting, $T_m$, and the glass transition temperature, $T_g$, are best known. In addition to these there are smaller ones detectable on the derivative properties, e.g., the compressibility and the thermal expansion coefficients ($\kappa$ and $\alpha$, respectively):

$$\kappa \equiv \left( \partial \ln V / \partial P \right)_{T,P^o,q} \qquad ; \quad \alpha \equiv \left( \partial \ln V / \partial T \right)_{T^o,P,q} \tag{3}$$

where $P^o$ and $T^o$ are solidification pressure and temperature, respectively, and $q$ is the rate of heating or compressing.

The first, quantum transition at $T <$ 80 K, was predicted by Simha *et al.* [16]. [16] Above, but at $T < T_g$ there are other glass-glass transitions, identified by the letters of Greek alphabet [17].[17] Of these $T_\beta \approx 0.8\ T_g$ is the most important as it limits the region of physical aging of vitreous materials [18].[18] Also at $T > T_g$ there are transitions such as the

cross-over transition, $T_c/T_g \approx 1.15 - 1.35$. The magnitude of this ratio was found dependent on the fragility index [19]:[19]

$$m = \left(\frac{1}{T_g}\right)\left(\frac{d\log\eta}{d\left(1/T\right)}\right)_{T=T_g} \quad (4)$$

The transition at $T_c$ is readily observed by neutron scattering and other vibrational spectra, in dielectric or rheological measurements, but not directly in *PVT.* The mode-coupling theory (MCT) considers liquid as an assembly of particles enclosed in cages formed by their neighbors with $\alpha$-relaxation controlling the behavior. Only at $T > T_c$ the molecular vibrations dominate. Götze and Sjogren wrote: "$T_c$ *seems to be an equilibrium parameter of the system, which separates the supercooled liquid state in two regions*" [20]*.* [20] Semi-crystalline polymers have a dual nature, in part being amorphous in part crystalline; in most $T_m \approx 1.5\ T_g$ [21].[21]

DETERMINATION OF *PVT*

The HPD is used for determining the *PVT* surface in $V = V(T, P)$ coordinates with accuracy of 0.0002 ml/g. The specimens are tested within the range of temperatures, $T$ = 300-590 K, and pressures, $P$ = 0.1 to 190 MPa. The measurements are automatic, either increasing or decreasing $T$ and $P$ in steps. Depending on the selected rate the measurement of 350 to 750 data points takes 16 to 36 h. The four procedures used for *PVT* tests are listed in Table IV.

Table IV. Procedures of *PVT* measurements

| Procedures | Constant variable | Adjusted variable |
|---|---|---|
| Isothermal heating ("standard") | $T$ is kept constant until $P$-sweep is completed, then increased to another level between the ambient and the maximum level, $T_{max}$. | $P$ increases from 10 to 200 MPa. |
| Isothermal cooling | Initially $T \approx T_g$ + 30 °C is constant until $P$-sweep is completed, then decreased to another level toward the ambient $T$ | $P$ increases from 10 to 200 MPa. |
| Isobaric heating | $P$ is kept constant until $T$-sweep is completed, then increased to another level between 10 and 200 MPa | $T$ increases from ambient to $T_{max}$. |
| Isobaric cooling | $P$ is kept constant until $T$-sweep is completed, then increased to another level between 10 and 200 MPa | $T$ decreases from $T \approx T_g$ + 30 °C to ambient |

*Note: As P increases the resulting adiabatic heating increases the set T by up to 5°C. In principle, the experiments may also be conducted reducing P.*

The "standard" and the isobaric cooling tests show large transitory regions below $T_g$. Only the isobaric heating in Figure 2 shows a regular behavior with nearly constant slopes (a measure of the thermal expansion coefficient, $\alpha$) in the vitreous and molten phase. Evidently, different procedures are used for different purpose. For example, the standard procedure guarantees that specimens see the highest temperature only at the end of the test, thus these measurements are not affected by the thermal degradation. The isobaric cooling from $T \approx T_g$ + 30 °C has been used for studying the thermodynamics of glass transition [22]. [22]

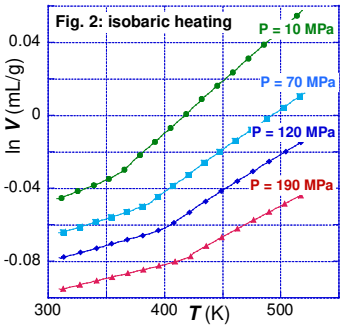


Figure 2. PVT dependence of polystyrene (PS) measured by isobaric heating. One-in-five points are shown.

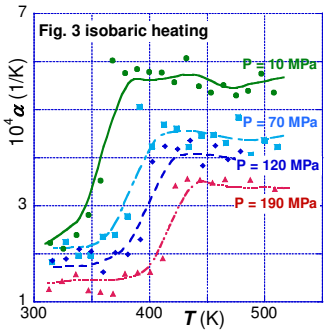


Figure 3. Volumetric thermal expansion coefficient vs. T, computed from data in Fig. 2.

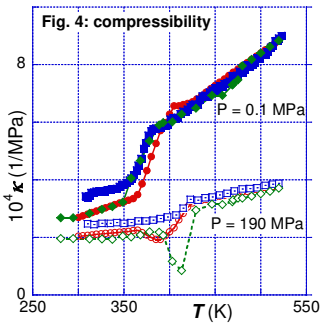


Figure 4. Compressibility vs. T determined by the standard method (circles), isobaric heating & cooling (squares & diamonds).

## EFFECTS OF CLAY, INTERCALANT AND COMPATIBILIZER

Since the expandable clay is hygroscopic containing ca. 7 wt% $H_2O$, CPNC samples must be vacuum dried [23].[23] Commercial organoclay contain up to 40 wt% excess of intercalant with relatively high free volume content that affects *PVT* behavior. Highly polar PA-6 strongly interacts with crystalline clays having high surface energy [24].[24] The interactions are so strong that PA-6 expels intercalant from clay surface and forms 4 – 6 nm thick solid layer of polymer, followed by about 100 nm thick layer of organic molecules with increasing mobility as the distance from the clay surface increases [25]. [25] The adsorption and solidification reduce the free volume by *ca.* 15%. In CPNC, polymer and organoclay are thermodynamically immiscible and must be compatibilized. The thermodynamics treat nano-sized clay platelets and polymeric macromolecules as statistical elements of the network, thus if exfoliation is required, system miscibility is needed. Since macromolecular diffusion into the clay galleries reduces the system entropy, $\Delta S < 0$, the miscibility might be expected only if the enthalpy is negative, $\Delta H < 0$, *i.e.,* if the specific interactions are strong [26].[26]

## DERIVATIVES; COMPRESSIBILITY AND THERMAL EXPANSION COEFFICIENT

The raw data that come from HPD usually have well defined, constant *P*-values, but because of adiabatic heating effects, *T* is different at each *P* level. Thus, if the derivatives $\alpha$ and $\kappa$ are required, one need to have evenly spaced data points at constant *T* and *P*. Three methods have been applied to accomplish this, viz., fitting the data to a polynomial, or the Tait equation [27, 28], [27, 28] but the best approach is an interpolation to the same *T*-value at *P* = *constant*. When the derivatives are used for detecting small transitions, only the interpolative method is acceptable [29].[29]

Numerical differentiation of dependencies displayed in Figure 2 leads to the temperature-dependent thermal expansion and compressibility coefficients presented in Figures 3 and 4, respectively. The simplest $\alpha$-dependencies were obtained by isobaric heating at a rate of 2°C/h. Figures 3 and 4 show that while the thermal expansion coefficient, $\alpha = \alpha(T)$ within the vitreous and molten phase varies little with *T*, the compressibility coefficient, $\kappa = \kappa(T)$ increases in both phases. Notably, in Figures 2 – 4 there is a weak evidence for the presence of $T_c$ transition at 475 ± 5 K. The heating or cooling rate in the vicinity of $T_g$ is important for the polymer structure and behavior on both sides of the transition temperature, related to the non-equilibrium fractal structures below $T_c$ [30, 31]. [30, 31]

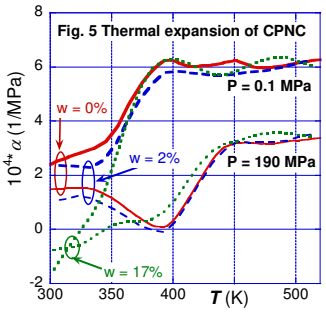


Figure 5. Temperature dependence of the volumetric thermal expansion coefficient at two pressures and four concentrations.

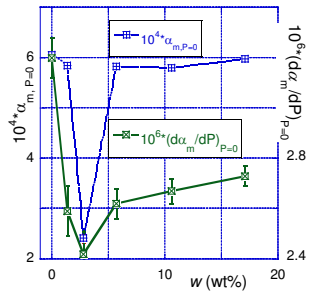


Figure 6. The thermal expansion coefficient at $T > T_g$ and its pressure gradient as function of clay concentration, w.

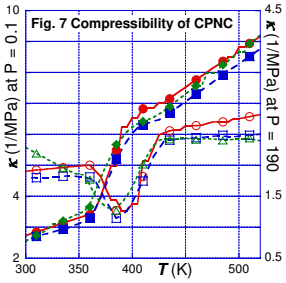


Figure 7. Compressibility coefficient vs. T at P = 0.1 and 190 MPa for PNC containing: w = 0, 2 and 17 wt%.

CPNC was melt compounded from PS-with 0 – 17.1 wt% of Cloisite®10A organoclay in a TSE [32-34].[32, 33, 34] The HPD data were obtained using the "standard" *PVT* isothermal heating procedure; Figures 5 and 6 display $\alpha$ as function of *P, T* and *w.* In the vitreous state $\alpha_g$ shows two types of behavior. For clay loadings $w \leq 2$ % it has low value decreasing with *P* to about zero, whereas for $w > 3.6$ wt% its values are negative, *i.e.*, heated specimen shrinks with *T* instead of expanding. The magnitude of $\alpha_g$ at $T < T_g$ strongly depends on the cooling process from the melt. In the molten state the isobaric values of $\alpha_m$ are nearly constant, independent of *T.* Addition of clay reduces $\alpha_g$ in the full range of *P.* In the vicinity of $w_2 = 3.6$ wt% the function takes a dip. A similar, but stronger local decrease is observed in the melt; Figure 6 displays $\alpha_m = \alpha_m(w)$ at ambient pressure and its pressure gradient. Figure 7 displays $\kappa$ as functions of *P, T* and *w.* By contrast with $\alpha$, the compressibility tends to increase with *T.* However, the temperature dependence of $\kappa$ decreases with *P* virtually to zero at the highest *P* and *w*. The $\kappa = \kappa(w)$ dependence also goes through a local minimum near $w_2 = 3.6$ wt%.

## EFFECT OF CLAY ON α AND κ IN PA-6 BASED PNC

Dry PA-6 has two transitions of interest: $T_g$(PA-6) ≈ 323 and $T_m$(PA-6) ≈ 500 K, both dependent on *P* as well as on the method of material preparation. The HPD measurements of PA-6, its PNC-2 and PNC-5 containing 2.29 ± 0.13 and 4.91 ± 0.24 wt% of clay, respectively (inorganic content), were carried out at $T = 300 – 580$ K and $P = 0.1 – 190$ MPa [35].[35] The derivatives $\alpha$ and $\kappa$ were computed by numerical differentiation of the *PVT* isobaric or isothermal dependencies. As shown in Figure 8, the attention focused on $T_m$ region and its variation with *P, T* and *w.* The thermal expansion coefficient for the crystalline phase of PA-6 and its PNCs is shown is separated from the melt by a "chimney-like" melting zone. The addition of clay reduces $\alpha$ of the solid phase, and increases its value in the melt. This behavior might be related to the presence of high crystallinity regions in the vicinity of the MMT high energy surface. By contrast with $\alpha$ the $\kappa = \kappa(T)$ function for PA-6 and its PNCs follows the same dependence on both sides of $T_m$, as theoretically predicted [36, 37].[36, 37] The low-*P* compressibility slightly increases with clay, seemingly related to the intercalant presence.

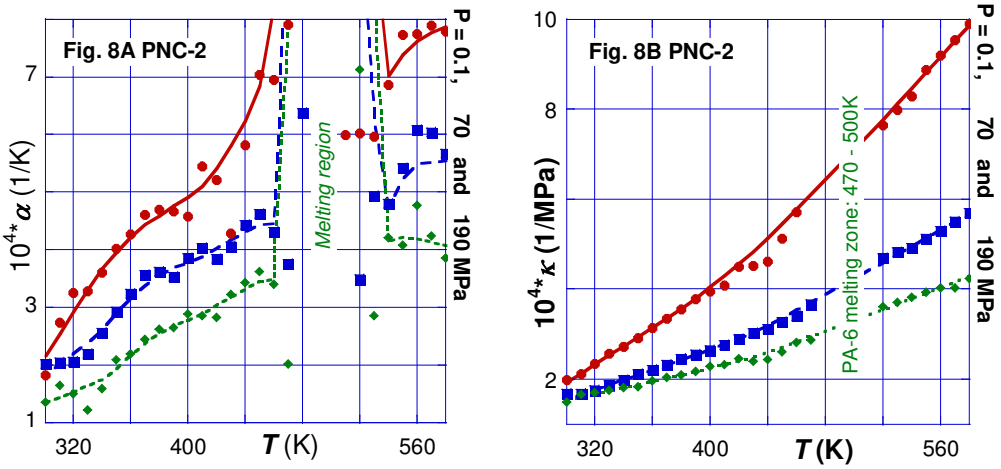


Figure 8A and 8B. The thermal expansion and compressibility coefficients vs. $T$ at P = 0.1 – 190 MPa for PA-6 nanocomposite with 2 wt% clay, PNC-2.

## THERMODYNAMIC THEORIES

The numerical calculation of $\alpha$ and $\kappa$ from the HPD data, on purpose did not involved any theoretical model. However, since an adequate theory may lead to determination of the interaction parameters, cohesive energy density, internal pressure, and the free volume content, a short discussion is justified. Furthermore, the theoretical analysis of CPNC behavior offers an insight into the non-equilibrium phenomena, such as diffusivity, rheology, positron annihilation lifetime spectroscopy (PALS), etc. [38]. [38]

### SIMHA-SOMCYNSKY CELL-HOLE THEORY

The Simha and Somcynsky (S-S) cell-hole theory is based on the lattice-hole model [39, 40].[39, 40] The molecular segments of $s$-mer occupy $y$-fraction of the lattice sites, while the remaining randomly distributed sites, $h = 1 - y$, are left empty accounting for the free volume. The theory was derived assuming thermodynamic equilibrium, later also postulating that at $T < T_g$ part of the free volume is frozen, what extended the theory to the vitreous and semi-crystalline non-equilibrium states [41].[41]

The derivation starts with the configurational partition function, which incorporates the Lennard-Jones (L-J) "6-12 potential" with two interaction parameters: the maximum attractive energy, $\varepsilon^*$, and the segmental repulsion volume, $v^*$. Next, assuming the corresponding states principle (CSP), the variables are divided by the characteristic reducing parameters:

$$\left.\begin{aligned}\tilde{V} &\equiv V / V^*\\ \tilde{T} &\equiv T / T^*\\ \tilde{P} &\equiv P / P^*\end{aligned}\right\} \Rightarrow \quad M_s \frac{P^* V^*}{R T^*} = \frac{c}{s} \quad \Leftarrow \left\{\begin{aligned}P^* &= zq\varepsilon^* / (sv^*)\\ T^* &= zq\varepsilon^* / (Rc)\\ V^* &= v^* / M_s\end{aligned}\right. \tag{5}$$

where $zq = s(z-2)+2$ is the number of interchain contacts between $s$ segments (each of molecular weight: $M_s = M_n/s$) in a lattice of the coordination number $z$, and $3c$ is the number of the external degrees of freedom. The reduced free volume function is a volume-average of the solid-like and gas-like contributions. From the configurational Helmholtz

free energy S-S derived the equation of state (eos), the cohesive energy density, $\widetilde{CED}$, solubility parameter, $\delta = \delta(T, P)$, and the internal pressure, $\tilde{p}_i$ [42-45]. [42, 43, 44, 45]

Next, the S-S theory for a single component liquid was extended to homogeneous, binary mixtures, postulating that there is only one type of vacancies and one cell size for the components [46, 47].[46, 47] The average interaction parameters $\langle \varepsilon^* \rangle$ and $\langle v^* \rangle$ are related to binary ones via:

$$\left\langle \varepsilon^* \right\rangle \left\langle v^* \right\rangle^m = \sum_{i,k} X_i X_k \varepsilon^*_{i,k} \left( v^*_{i,k} \right)^m ; \quad m \in (2,4) \tag{6}$$

where the two values of $m$ reflect the assumed Lennard-Jones 6-12 potential. The S-S theory for multicomponent systems well describes the phase equilibria, CED, solubility as well as *PVT* behavior of polymer mixtures with gases, liquids [48][48], solids [49-51] [49, 50, 51] and nanocomposites [52, 53]. [52, 53].

Figures 8A and 8B illustrate the effect of clay content on the free volume parameter $h$ and the L-J interaction parameters in molten PNC with PS matrix. At constant clay loading of 2 wt% adsorption-&-solidification of polymer linearly reduces the free volume content with the interlayer spacing, $d_{001}$ [32]: [32]

$$\Delta h = 2.51 + 0.833 d_{001} ; \quad r = 1.000 \tag{7}$$

Because of the favorable thermodynamic interactions between clay and PA-6 these CPNCs are exfoliated, at 2 wt% clay $h$ is reduced by 15%. The functions: $h$, $\langle \varepsilon^* \rangle$ and $\langle v^* \rangle$ *vs.* $w$ go through a local extrema at $w_2$ = 3.6 wt% clay – further addition of organoclay reduces the interlayer spacing and dilutes the intercalated stacks. The effect parallels the behavior of derivative properties on clay content shown in Figures 6 and 7.

The old notion of structure in molten polymers is being accepted on the theoretical and experimental evidences. The twinkling fractal theory (TFT) of the glass transition and recent atomic force microscopy (AFM) in the tapping-mode [54, 55] [54, 55] are convincing proofs of the dynamic, solid aggregate presence below and above $T_g$– only above the crossover temperature, $T_c$, the true liquid-like behavior was found. The detailed analysis of data from HPD, as well as dynamic shear tests of PS indicate the presence of a transient structure on both sides of $T_g$; hence, molten polymer not always is at the thermodynamic equilibrium. For example, the difference of rigidity in quenched and annealed specimens was detectable at $T \geq T_g + 20^oC$, i.e., half way to $T_c$ = 419 ± 2 K, or $T_c/T_g$ = 1.16 ± 0.01.

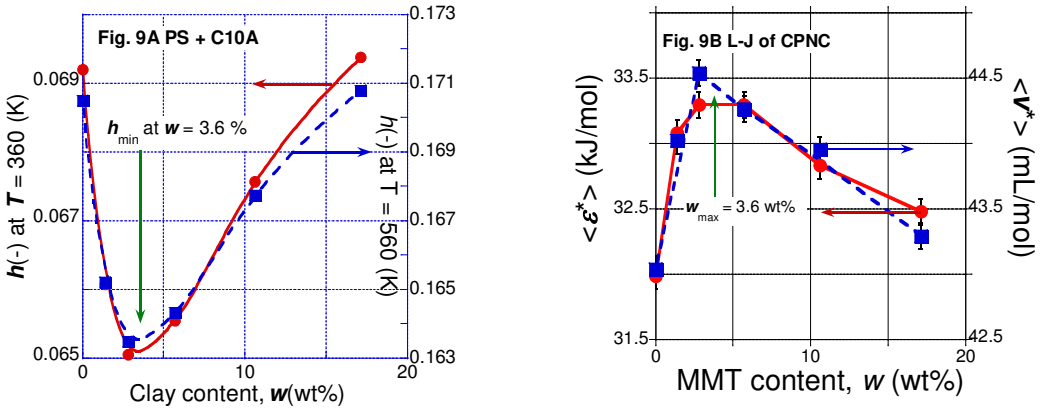


Figure 9A and 9B. Free volume and the L-J interaction parameters (Figure 9B) vs. clay content for PS-based CPNC at P = 0.1 MPa and T = 360 and 560 (K).

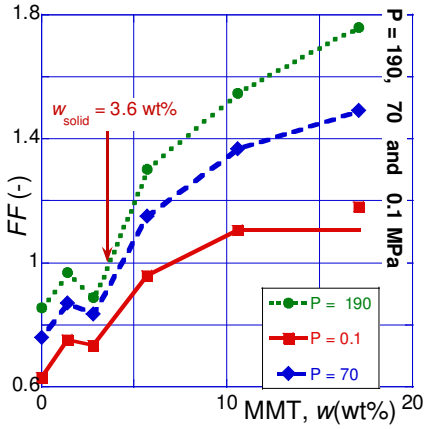


Figure 10. Free volume frozen fraction, FF = FF(w), for PS-1301 with 0 – 17 wt% of C10A at the selected (for clarity) five pressures, P = 0.1 – 190 MPa. See text.

Analysis of the *PVT* surface by means of the S-S eos leads to the hole content, *h*, which should correlate with liquids viscosity following the dependence [56-59]: [56, 57, 58, 59]

$$\ln \eta_{\sigma_{ij}=const} = a_0 + a_1 Y_s; \quad Y_s \equiv 1/(h + a_2) \tag{8}$$

The relation was found valid for low molecular weight *n*-paraffins or silicon oils within the ranges of $T$ = 20 to 204°C and $P$ = 0.1 to 500 MPa, with constants: $a_1$ = 0.79 ± 0.01 and $a_2$ = 0.07. However, it failed when applied to data of eight molten polymers, whose *PVT* and $\eta = \eta(P, T)$ were measured [60]. [60] The discrepancy is related to the presence of structures in the latter systems at $T_g \leq T \leq T_c \approx T_{LL}$. The presence of structures within this temperature range was postulated by Boyer and his colleagues; only above $T_{LL}$ the processing would yield articles with smooth surface and good, reproducible performance [61-62]. [61, 62]

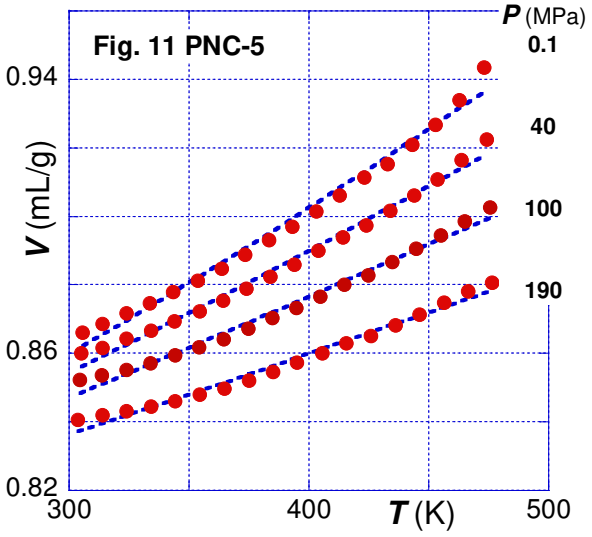


Figure 11. Specific volume of PA-6 with 5 wt% clay at P = 0.1 – 190 MPa. Points are experimental and lines computed from the Midha – Nanda –Simha-Jain (MNSJ) theory.

## THE VITREOUS REGION

Properties of the vitreous phase depend on the way it was achieved [63].[63] The analysis followed the procedure developed by Simha and his colleagues [64-66].[64, 65, 66] Accordingly, the frozen fraction of free volume, *FF*, was computed from the relation:

$$FF = 1 - \left(\partial h / \partial T'\right)_{P,glass} \Big/ \left(\partial h / \partial T'\right)_{P,extrapol} \leq 1 \tag{9}$$

Figure 10 displays the $FF = FF(w)$ dependence of CPNC = PS + C10A at several pressures. Only at $w < w_2 = 3.6$ wt%, $FF < 1$ is found, while at higher clay concentration $FF > 1$. This behavior stems from the adsorption-&-solidification of the CPNC samples during melt quenching from $T > T_g + 50^oC$.

## MNSJ EQUATION OF STATE FOR SEMI-CRYSTALLINE CPNC

Thermodynamic theory for semi-crystalline polymeric systems borrows from several sources: the quantum theory of polymeric glasses at $T \leq 80$ K [16], cell model for crystalline polymers [67]67, and several later refinements [68, 69]. 68, 69 The cell lattice does not have holes, thus the reducing parameters ($P^*$, $T^*$, $V^*$) are different than those computed using S-S eos cell-hole theory for equilibrium liquids. The theory is valid for the crystalline phase at $T_g \leq T\,(\mathrm{K}) \leq T_m$. The applicability for describing the *PVT* dependencies has been examined first for neat PE and PA-6 and then to CPNC. For the PA-6 systems the additivity of the crystalline and non-crystalline domains was assumed [35-37].[35, 36, 37] The sequence of the computation steps and the assumed models are detailed in the original publications. Figure 11 displays the final fit of the theory to HPD data.

## INTERACTION COEFFICIENTS

The L-J potential with adjustable exponents: $m = 10 - 13$, $n = 6 - 7$ was cast into the present form of the "6-12 potential" after the quantum mechanics showed that the attractive forces between hydrogen atoms follow with $n = 6$, and the repulsive interactions with $m = 2n$ [70].[70] The 6-12 potential was incorporated into the S-S and MNSJ theories. The single component, intersegmental L-J interaction parameters are $\varepsilon^*$ and $v^*$, whereas those for multi-component systems are averages, $\langle \varepsilon^* \rangle$ and $\langle v^* \rangle$. For extracting the individual binary interactions from these latter ones a model is needed.

The situation is relatively simple for the single-phase polymeric systems or even for immiscible binary polymer blends, where properties of each component directly can be measured, and only the heterogeneous ones, $\varepsilon^*_{ij}$ and $v^*_{ij}$ (i.e., polymer-i with polymer-j), must be determined from the blend behavior. It is noteworthy that such a treatment ignores the presence of the interphase whose importance increases with the enhanced dispersion [71]. [71]

CPNCs are more complex systems than blends as they comprise matrix, nano-sized particles, intercalant, compatibilizer(s) and various industrial additives. Furthermore, the clay usually exists in a wide spectrum of dispersion ranging from fully exfoliated to micron-size aggregates. Clay also adsorbs the organic phase creating a gradient of molecular mobility stretching up to 120 nm from the clay surface. During the last 20 years CPNCs with immiscible polymer blends became of interest [72]. [72] Thus, it is a challenge to convert these systems into a model mixture of matrix and dispersed in it solid particles that will realistically simulate the physical behavior.

The CPNC model should specify the composition of the matrix and dispersed solid phase. For computations, the solid particles are made off clay platelets with $z_1 \approx 4$–6 nm thick, solidified organic having the interaction parameters $\varepsilon^*_{22}$ and $v^*_{22}$. The remaining materials comprising the organic layer at $z > z_1$ must be treated as a matrix with $\varepsilon^*_{11}$ and $v^*_{11}$. In consequence, the model implicitly assumes that the L-J parameters depend on the clay content, limited to the low clay content, $w < w_2 = 3.6$ wt% [53].

Because of differences in clay-polymer interactions, one should not assume that a single model will be applicable to all CPNC. For example, owing to polarity of PA-6 and strong interaction with negatively charged clay platelets, the PA-6 based CPNC are relatively easily exfoliated by the synthetic or compounding method. However, since the intercalant location and molecular structure are different than that observed in PS or polyolefin (PO) matrix, the model for extracting the L-J parameter should account for the difference [15]. Flow analysis of the PA-6 based CPNC led to the "hairy clay particles" (HCP) model [73]. [73] By contrast, the ones with polyolefin (PO) or PS matrix, which does not bond to clay surface, are immiscible with most intercalants and need compatibilizer. In conclusion, before devising a realistic model for tested PNC, information about composition, thermodynamic interactions and degree of dispersion is needed [52].

For CPNCs out of the six parameters only two ($\varepsilon_{11}^*$ and $v_{11}^*$) can be measured directly. The two cross-interaction parameters, $\varepsilon_{12}^*$ and $v_{12}^*$, are calculated following the Berthelot's rule and the algebraic average, respectively:

$$\varepsilon_{12}^* = \left(\varepsilon_{11}^* \varepsilon_{22}^*\right)^{1/2} \quad and \quad v_{12}^* = \left[v_{11}^{*1/3} + v_{22}^{*1/3}\right]^3 \Big/ 8 \tag{10}$$

The remaining two parameters, $\varepsilon_{22}^*$ and $v_{22}^*$, are then calculable from average interaction expressions.

Figure 12 displays the concentration dependence of $\varepsilon_{22}^*$ for PS-based CPNC. The broken line represents the dependence with the expected maximum at the critical concentration, $w_2$ = 3.6 wt% [52]. Figure 13 shows the concentration dependence of the computed binary interaction parameters in the full range of clay content, $w$ = 0 – 100 wt% for PP-based CPNC with C20A. The computations lead to $\varepsilon_{11}^*$ and $v_{11}^*$ for all points, excepting the two last ones at $w$ = 100 wt% clay corresponding to $\varepsilon_{22}^*$ and $v_{22}^*$. From these two sets of numbers the cross-interactions, $\varepsilon_{12}^*$ and $v_{12}^*$, may be calculated.

The theory also suggests that the L-J parameters may not be independent, viz. $\varepsilon^* \propto v^* P^*$ [45]. The empirical relation for PS and its CPNC is: $\varepsilon^* \cong 13.4 + 0.445 v^*; r = 0.95$.

The binary interaction parameters for the matrix ($\varepsilon_{11}^*$, $v_{11}^*$) and for the solid phase ($\varepsilon_{22}^*$, $v_{22}^*$) are listed in Table V. It may seem odd that the difference between the interaction parameters of the matrix and solid part is so small. However, the definition of solids is a clay platelet enrobed with an organic phase, thus there are no clay-clay interactions, but rather those between polymeric solid layers adsorbed on the clay platelets and the polymeric matrix.

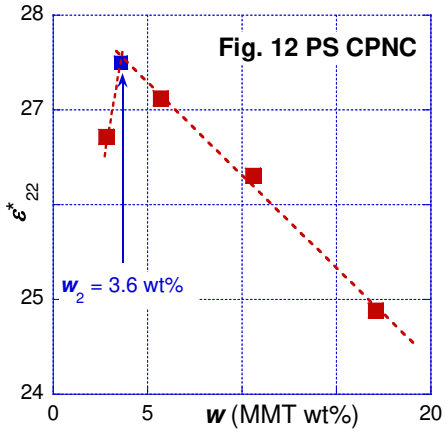


Figure 12. Computed stack-stack interaction for intercalated PS-based CPNC.

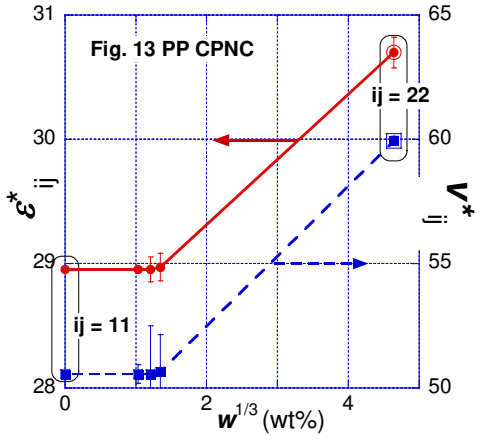


Figure 13. L-J interaction parameters for PP-based CPNC.

Table V. The binary interaction parameters for PNC with PA-6, PP and PS matrix.

| Polymer | Matrix | | Solid | | Refs. |
|---|---|---|---|---|---|
| | $\varepsilon_{11}^*$ | $v_{11}^*$ | $\varepsilon_{22}^*$ | $v_{22}^*$ | |
| PA-6 | 34.1 ± 0.3 | 32.0 ± 0.1 | 31.2 ± 0.3 | 25.9 ± 0.3 | [35] |
| PP | 28.9 ± 0.1 | 50.6 ± 0.4 | 30.7 ± 0.4 | 59.9 ± 0.3 | [53] |
| PS | 32.0 ± 0.6 | 43.0 ± 1.7 | 33.0 ± 0.1 | 44.2 ± 0.1 | [52] |

## THEORETICAL PREDICTIONS

Theories are built assuming that on the one hand they should simulate the phenomenon and on the other permit comparison with experimental results. The notorious assumption in the polymer theories is an omission of polydispersity, the presence of additives and the non-random distribution of properties, *e.g.*, introduced by mixing or temperature gradients. Furthermore, the thermodynamics theories usually assume equilibrium within a single phase.

The S-S and MNSJ equations of state predict the *PVT* variability of, respectively, amorphous and semi-crystalline molten polymer and the $\alpha$ and $\kappa$ derivatives. The theories are cast in reduced form, thus they are universally applicable to any system with known set of the reducing parameters, $P^*$, $T^*$ and $V^*$ (viz. eq. 5). Figures 14A and 14B show, respectively, the $\alpha$ and $\kappa$ dependencies for PA-6 at, e.g., $T$ = 5 – 284°C, $P$ = 25 – 314 MPa, $10^4\alpha$ = 3.35 – 8.02 (1/K) and $\kappa$ = 0.13 – 1.01 (1/kPa); these values are well within the experimental magnitudes of these coefficients. Similarly good representation of the experimental data was obtained for PS at $T$ = 20 – 313°C, $P$ = 11 – 189 MPa, where $10^4\alpha$ = 3.52 – 8.44 (1/K) and $\kappa$ = 0.07 – 0.60 (1/kPa).

The S-S eos well describes the *PVT* behavior of amorphous polymers up to the second volume derivatives. The experimental PA-6 data were compared with a theoretical model assuming dispersion of PA-6 crystals in its melt. Accordingly, the applied MNSJ and S-S theories, respectively, showed excellent agreement with the experimental data.

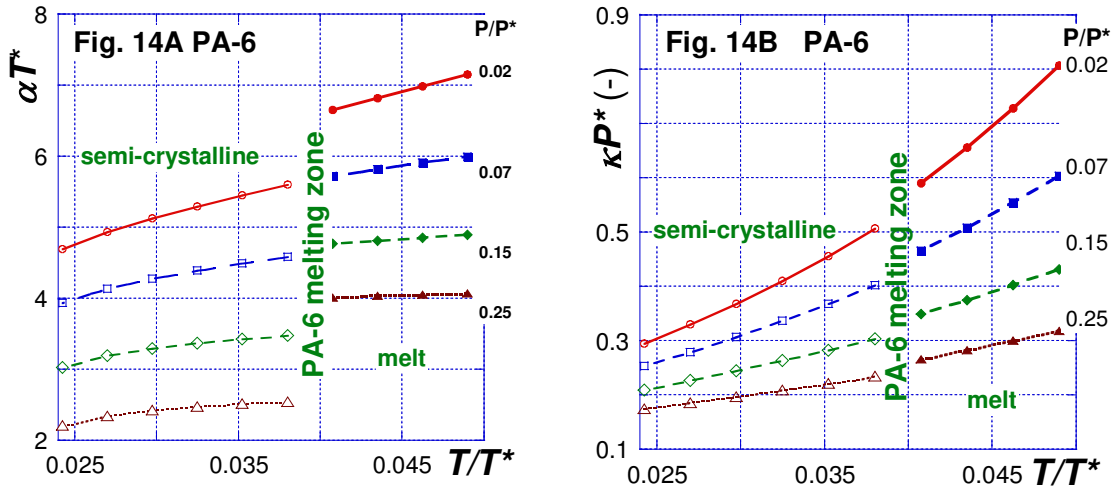


Figure 14A and 14B. Theoretical predictions of the thermal expansion and compressibility coefficients in reduced variables for a semi-crystalline/molten polymeric system computed from a combination of S-S and MNSJ eos [36, 37]. [36, 37]

## SUMMARY AND CONCLUSIONS

This presentation discussed three aspects of CPNC:

- *Characterization of clays*
- *HPD measurements, thermodynamic theories and binary interactions*
- *The non-equilibrium structures on both sides of $T_g$.*

The natural clays significantly vary with the geographical location and local mine strata. The differences are in: platelet shape, size and size distribution, chemical composition and the presence of organic and inorganic contaminants.

Of the four HPD test procedures the most useful is the isobaric heating method, while the "standard" isothermal compression is useful for the thermally unstable systems. The *PVT* data should be directly numerically differentiated for $\alpha$ and $\kappa$ coefficients. Amorphous and semi-crystalline *PVT* data well follow the S-S and MNSJ theories, respectively. Comparison of the theoretical predictions with the experimental plots of the $\alpha$ and $\kappa$ variation with $T$ and $P$ show good agreement up to the second derivative. For CPNC, the analysis of the HPD data by means of these theories leads to the determination of the binary matrix-clay L-J interaction parameters.

Finally, the demonstrated non-equilibrium nature of polymeric systems on both sides of $T_g$ demands caution while generalizing the result; a significant difference in melt behavior was observed by varying the time scale of the experiment.

## REFERENCES


1 Utracki, L. A. 2004. *Clay-Containing Polymeric Nanocomposites*, RAPRA, Shawbury, UK. ISBN: 978-1-85957-488-1

2 Utracki, L. A., M. Sepehr and J. Li. 2006. "Melt compounding of polymeric nanocomposites," *Intern. Polym. Process.*, 21(1): 1 – 14.

3 Utracki, L. A., M. Sepehr, and E. Boccaleri. 2007. "Synthetic, layered nano-particles for polymeric nanocomposites (PNC's)," *Polym. Adv. Technol.*, 18(1): 1–37. DOI: 10.1002/pat.852

4 Utracki, L. A., W. Broughton, N. Gonzalez Rojano, L. Carvalho, and C. A. Achete. 2011. "Clays for polymeric nanocomposites," *Polym. Eng. Sci.*, 51(4): 559–572. DOI 10.1002/pen.21807.

5 Clarey, M., J. Edwards, S. J. Tsipursky, G. W Beall. and D. D. Eisenhour, Method of manufacturing polymer - grade clay for use in nanocomposites, US Pat., 6,050,509, 18.04.2000.

6 Utracki, L. A. Ed., 2002. *Polymer Blends Handbook*, Kluwer, Dordrecht. ISBN: 978-0-306-48244-1

7 Song, W., 2000. "Comprehensive study of a new extensional flow mixer," *SPE ANTEC, Techn. Pap*. 46(1): 270-275.

8 Israelachvili J. N., M. Tirrell, J. Klein and Y., Almog. 1984. "Forces between two layers of adsorbed polystyrene immersed in cyclohexane below and above the Θ-temperature," *Macromolecules*, 17(2): 204 – 209.

9 Horn, R. G. and J. N. Israelachvili. 1988. "Molecular organization and viscosity of a thin film of molten polymer between two surfaces as probed by force measurements," *Macromolecules*, 21(9): 2836 – 2841.

10 Cosgrove T., T. G. Heath, K. Ryan and T. L. Crowley. 1987. "Neutron scattering from adsorbed polymer layers," *Macromolecules*, 20(11), 2879 – 2882.

11 Cosgrove T., T. G. Heath, T. J. S. Phipps and R. M. Richardson. 1991. "Neutron reflectivity studies of polymer adsorbed on mica from solution," *Macromolecules*, 24(1): 94 – 98.

12 Fleer G., M. A. Cohen-Stuart, J. M. H. M. Scheutjens, T. Cosgrove and B. Vincent. 1993. *Polymers at Interfaces*, Chapman and Hall, London.

13 Hentschke R. 1997. "Molecular modeling of adsorption and ordering at solid interfaces," *Macromol. Theory Simul.*, 6(2): 287 – 316.

14 Termonia Y. 2009. "Monte Carlo modeling of dense polymer melts near nanoparticles," *Polymer*, 50(4): 1062 – 1066.

15 Tokihisa M., K. Yakemoto, T. Sakai, L. A. Utracki, M. Sepehr, J. Li and Y. Simard, 2006. "Extensional Flow Mixer for Polymer Nanocomposites," *Polym. Eng. Sci*. 46(8): 1040–1050; DOI 10.1002/pen.20542

16 Simha R., J. M. Roe and V. S. Nanda. 1972. "Low-temperature equation of state for amorphous polymer glasses," *J. Appl. Phys.*, 43: 4312 – 4317.

17 Boyer R. F. 1980. "Dynamics and thermodynamics of the liquid state T > Tg of amorphous polymers." *J Macromol Sci. – Phys.*, B183: 461 – 553; Boyer R. F. 1987. "Evidence from $T_{LL}$ and related phenomena for local structure in the amorphous state of polymers," in *Order in the amorphous state*, R. L. Miller and J. K. Rieke, eds. New York: Plenum.

18 Struik L. C. E. 1978, *Physical aging in amorphous polymers and other materials*. Amsterdam: Elsevier.

19 Surovtsev N. V. 2007. "Interrelation between fast relaxation and mode-coupling theory temperature in glass formers," *J. Phys.: Condens. Matter.*, 19, 196101 (8 pp).

20 Götze W., L. Sjogren 1992. "Relaxation processes in supercooled liquids," *Rep. Prog. Phys.*, 55: 241-370.

21 Boyer R. F. 1985. "$T_{LL}$ and related liquid state transitions-relaxations: A review," in *Polymer Yearbook 2*, R, A. Pethrick, ed., Chur-London-Paris-New York: Harwood Academic Publishers.

22 Quach A. and R. Simha. 1971. "Pressure-volume-temperature properties and transitions of amorphous polymers; polystyrene and poly(o-methyl-styrene)," *J. Appl. Phys.*, 42, 4592 – 4606; Quach A. and R. Simha. 1972. "Statistical thermodynamics of the glass transition and the glassy state of polymers," *J. Phys. Chem.*, 76: 416 – 421.

23 Utracki L. A., R. Simha and A. Garcia-Rejon, 2003. "Pressure-Volume-Temperature relations in nanocomposite," *Macromolecules*, 36(6), 2114 – 2121.

24 Tanaka G. and L. A. Goettler, 2002. "Predicting the binding energy for nylon 6,6/clay nanocomposites by molecular modeling," *Polymer*, 43(2), 541-553.

25 Luengo G., F.-J. Schmitt, R. Hill and J. N. Israelachvili, 1997. "Thin film rheology and tribology of confined polymer melts: contrasts with bulk properties," 30(8), 2482 – 2494.

26 Kim K., L. A. Utracki and M. R. Kamal, 2004. "Numerical simulation of polymer nanocomposites using a self-consistent mean-field model," *J. Chem. Phys.*, 121, 10766 - 10777.

27 Tait P. G. 1889. "On some of the physical properties of fresh water and of sea-water," in *Report on the Scientific Results of the Voyage of H.M.S. Challenger*, Thomson C. W., ed., Physics and Chemistry, 2(IV), 1.

28 Nanda V. S. and R. Simha. 1964. "Theoretical interpretation of Tait equation parameters," *J. Chem. Phys.*, 41, 1884 – 1885.

29 Utracki, L. A. 2012. "PVT Characterization of polymeric nanocomposites," Chapter 2 in *Characterization Techniques of Polymer Nanocomposites*, V. Mittal, Ed., Wiley VCH Verlag, Weinheim, Germany.

30 Wool R. P. 2008. "Twinkling fractal theory of the glass transition," *J Polym Sci. Part B Polym Phys.,* 46:2765–2778.

31 Utracki, L. A. and P. Sammut. 2011. "Molten Polystyrene Structures Above the Glass Transition, T > Tg," J*. Polym. Sci. Part B: Polym. Phys*., 49, 000–000; DOI: 10.1002/polb.22313.

32 Tanoue S., L. A. Utracki, A. Garcia–Rejon, J. Tatibouët, K. C. Cole and M. R. Kamal. 2004. "Melt compounding of different grades of polystyrene with organoclay: Part 1. Compounding and characterization," *Polym. Eng. Sci*., 44(6), 1046 – 1060.

33 Tanoue S., L. A. Utracki, A. Garcia–Rejon, P. Sammut, M.-T. Ton-That, I. Pesneau, M. R. Kamal and J. Lyngaae-Jørgensen. 2004. "Melt compounding of different grades polystyrene with organoclay: Part 2. Rheological properties," *Polym. Eng. Sci*., 44(6), 1061 – 1076.

34 Tanoue S., L. A. Utracki, A. Garcia–Rejon, J. Tatibouët and M. R. Kamal. 2005. "Melt compounding of different grades of polystyrene with organoclay: Part 3. Mechanical properties," *Polym. Eng. Sci*., 45(6), 827 – 837.

35 Utracki L. A. 2009. "Equation of state of polyamide-6 and its nanocomposites: 1. Fundamentals and the matrix," *J. Polym. Sci. Part B: Polym. Phys*., 47(3), 299 -- 313; "2. Effects of clay", *J. Polym. Sci. Part B: Polym. Phys*., 47(10), 966–980.

36 Utracki L. A. 2009. "Compressibility and thermal expansion coefficients of nanocomposites with amorphous and crystalline polymer matrix," *European Polym J.,* 45(7), 1891–1903.

37 Utracki L. A. 2010. "PVT of amorphous and crystalline polymers and their nanocomposites," *Polym. Degradation Stability*, 95(3), 411–421.

38 Utracki L. A. and A. M. Jamieson, eds. 2010. *Polymer Physics: From Suspensions to Nanocomposites to Beyond*, New York: J. Wiley & Sons.

39 Simha R. and T. Somcynsky. 1969. "On the statistical thermodynamics of spherical and chain molecule fluids," *Macromolecules*, 2(4): 342 – 350.

40 Somcynsky T. and R. Simha. 1971. "Hole theory of liquids and glass transition," *J. Appl. Phys*., 42: 4545 – 4548.

41 Jain R. K. and R. Simha. 1979. "High-pressure isotherms of polyethylene crystals," *J. Polym. Sci.: Polym. Lett. Ed*., 17(1): 33 – 37.

42 Utracki L. A. 2004. "Statistical thermodynamics evaluation of solubility parameters and polymer miscibility," *J Polym Sci. Part B: Polym Phys*., 42(15): 2909 – 2915.

43 Utracki L. A. and R. Simha. 2004. "Statistical thermodynamics predictions of the solubility parameter," *Polym. Int.,* 53(3): 279 – 286.

44 Utracki L. A. and R. Simha. 2001. "Free volume and viscosity of polymer-compressed gas mixtures during extrusion foaming," *J. Polym. Sci.: Part B: Polym. Phys*., 39(3): 342 – 362

45 Utracki L. A. 2005. "Pressure-Volume-Temperature dependencies of polystyrenes," *Polymer*, 46(25): 11548 – 11556.

46 Jain R. K. and R. Simha. 1980. "On the statistical thermodynamics of multicomponent fluids: equation of state," *Macromolecules*, 13(6): 1501 – 1508.

47 Jain R. K. and R. Simha. 1984. "Statistical thermodynamics of multicomponent fluids," *Macromolecules*, 17(12): 2663 – 2668.

48 Utracki L. A. and R. Simha. 2001. "Analytical representation of solutions to lattice-hole theory," *Macromol. Theory Simul*., 10(1): 17 – 24.

49 Simha R., R. K. Jain and S. C. Jain. 1984. "Bulk modulus and thermal expansivity of melt polymer composites: statistical versus macro - mechanics," *Polym. Compos.*, 5(1): 3 – 10.

50 Papazoglou E., R. Simha and F. H. J. Maurer. 1989. "Thermal expansivity of particulate composites: interlayer versus molecular model," *Rheol. Acta*, 28(4): 302 – 308.

51 Simha R., E. Papazoglou and F. H. J. Maurer. 1989. "Thermal expansivity and bulk modulus of polymer composites: experiment versus theory," *Polym. Compos.*, 10(6): 409 – 413.

52 Utracki L. A., 2008. "Free volume of molten and glassy polystyrene and its nanocomposites," *J. Polym. Sci. Part B: Polym. Phys.*, 46(23): 2504 – 2518.

53 Utracki L. A. and R. Simha. 2004. "Pressure-Volume-Temperature Dependence of Polypropylene/ Organoclay Nanocomposites," *Macromolecules*, 37(26): 10123 – 10133.

54 Wool R. P. and A. Campanella. 2009. "Twinkling fractal theory of the glass transition: Rate dependence and time–temperature superposition, in polymers," *J. Polym. Sci. Part B: Polym. Phys.*, 47(24): 2578–2590.

55 Stanzione III J. F., K. E. Strawhecker and R. P. Wool. 2011. "Observing the twinkling fractal nature of the glass transition," *J. Non-Crystalline Solids*, 357(2): 311-319, doi: 10.1016/j.jnoncrysol.2010.06.041.

56 Utracki L. A. 1983. "Pressure dependence of Newtonian viscosity," *Polym Eng Sci.*, 23(8): 446 – 452.

57 Utracki L. A. 1983. "Temperature and pressure dependence of liquid viscosity," *Canad. J. Chem. Eng.*, 61(5): 753 – 758.

58 Utracki L. A. 1986. "Correlation between PVT behavior and the zero – shear viscosity of liquid mixtures," *J. Rheol.*, 30(4): 829 – 841.

59 Utracki L. A. 1985. "A Method of Computation of the pressure effects on melt viscosity," *Polym Eng Sci.*, 25(11): 655 – 668.

60 Utracki L. A. and T. Sedlacek. 2007. "Free volume dependence of polymer viscosity," *Rheologica Acta*, 46(4): 479–494; DOI 10.1007/s00397-006-0133-z.

61 Stadnicki S. J. and J. K. Gillham. 1976. "The Tll (> Tg) transition of atactic polystyrene," *J. Appl. Polym. Sci.*, 20(5), 1245 – 1275.

62 Keinath, S. E.; Boyer, R. F. 1981. "Thermomechanical analysis of $T_g$ and $T > T_g$ transitions in polystyrene," *J. Appl. Polym. Sci.*, 26(6), 2077 – 2085.

63 Schmidt M. 2000. *Macroscopic volume and free volume of polymer blends and pressure-densified polymers*. Ph.D. Thesis, Chalmers University, Göteborg.

64 McKinney J. E. and R. Simha. 1974. "Configurational thermodynamic properties of polymer liquids and glasses. Poly(vinyl acetate)." *Macromolecules*, 7(6), 894 – 901; ibid., 1976. 9, 430 – 441; 1977. *J Res NBS – Phys Chem*, 81A, 283 – 297.

65 Curro J. G., R. R. Lagasse and R. Simha. 1981. "Use of a theoretical equation of state to interpret time-dependent free volume in polymer glass," *J. Appl. Phys.*, 52(10), 5892 – 5897.

66 Utracki L. A. 2007. "Pressure-Volume-Temperature of molten and glassy polymers," *J. Polym. Sci. Part B: Polym. Phys.*, 45(3), 270 – 285.

67 Midha, Y. R. and V. S. Nanda. 1977. "Equation of state for a polymer crystal," *Macromolecules*, 10(5), 1031 – 1035.

68 Simha R. and R. K. Jain. 1978. "Statistical Thermodynamics of Polymer Crystal and Melt," *J. Polym. Sci. Part B: Polym. Phys. Ed.*, 16(8): 1471 – 1489.

69 Jain R. K. and R. Simha. 1979. "Equation of state of semicrystalline and crystalline polymers," *J. Polym. Sci.: Polym. Phys. Ed.*, 17(11), 1929 – 1946.

70 Lennard-Jones J. E. and A. F. Devonshire. 1937. "Critical phenomena in gases I.", *Proc. Roy. Soc.*, 163(1), 53 – 70.

71 Utracki L. A. 1989. *Polymer Alloys and Blends*, Munich: Hanser Verlag; Utracki L. A., Ed. 2002. *Polymer Blends Handbook*, Dordrecht: Kluwer Academic Pub.

72 Utracki L. A. 2011. "Rheology of Polymer Blends," in *Encyclopedia of Polymer Blends*, Chapter 2, Volume 2, A. Isayev, Ed., Weinheim: Wiley-VCH Verlag.

73 Utracki L. A. and J. Lyngaae-Jørgensen. 2002. Dynamic melt flow of nanocomposites based on poly-ε-caprolactam," *Rheologica Acta*, 41(5), 394 – 407.